Modeling the Facet Growth Rate Dispersion of β L-Glutamic Acid – Combining Single Crystal Experiments with nD Particle Size Distribution Data

David R. Ochsenbein[a], Stefan Schorsch[b], Fabio Salvatori[b], Thomas Vetter[c], Manfred Morari[a], Marco Mazzotti[b,*]

[a] *ETH Zurich, Automatic Control Laboratory, Physikstrasse 3, CH-8092 Zurich, Switzerland*
[b] *ETH Zurich, Institute of Process Engineering, Sonneggstrasse 3, CH-8092 Zurich, Switzerland*
[c] *University of Manchester, School of Chemical Engineering and Analytical Science, M13 9PL Manchester, United Kingdom*

Abstract

The growth rate dispersion of needle-like β L-glutamic acid in the length direction is measured using a stagnant solution hot stage microscopy setup. Possible causes of the observed dispersion are analyzed and the resulting distribution of growth rates is used to motivate and reconstruct a distribution of an internal, growth affecting property of the crystals. The latter is then used as the initial condition for a multidimensional, morphological population balance model, whose outputs are fitted to 2D particle size distribution measurements obtained from seeded batch desupersaturation experiments. It is shown, through analysis of both types of data, that a non-zero rate of change in the direction of the new coordinate is required and a phenomenological description of this rate is proposed. The resulting model is able to quantitatively describe experimental data obtained from independent measurement devices, operating at different scales simultaneously.

Keywords: Crystallization, Crystal Shape, Crystal Growth, Growth Rate Dispersion, Morphological Population Balance Modeling, Hot Stage Microscopy

*Corresponding author: phone +41 44 632 2456; fax +41 44 632 11 41.
Email address: marco.mazzotti@ipe.mavt.ethz.ch (Marco Mazzotti)

1. Introduction

Crystallization is a ubiquitous purification step in the fine chemical and pharmaceutical industry. Beside the all-important chemical purity, the distribution of particle sizes and shapes is an important property of the particulate system that determines product quality due to its strong influence on downstream processes. Nevertheless, it is only with recent advancements of imaging tools and computational techniques, that the measurement and modeling of particle size and shape distributions (PSSDs) has become more accessible (Wang et al., 2007, 2008; Singh and Ramkrishna, 2013; Schorsch et al., 2012, 2014; Schorsch, 2014), allowing for parameter estimation of face-specific growth rates (Ma and Wang, 2012; Borchert et al., 2014; Ochsenbein et al., 2014) and eventually shape control. The continued progress of these technologies further enables gaining unprecedented insight into the mechanisms affecting the size and shape of crystals, thereby creating the possibility of studying crystallization processes on a more fundamental level.

An interesting topic of research in which–historically–imaging methods have been of great importance, is that of growth rate dispersion (GRD). Indeed, the discovery and subsequent investigation of the fact that a number of (in)organic crystal systems exhibit large variations of their growth rate has heavily relied on these techniques. Growth rate dispersion may be present both in the temporal domain, i.e., a single crystal's growth rate may fluctuate over time, as well as within a population of crystals, i.e., crystals exhibit different growth rates when exposed to identical experimental conditions even when they have the same size and shape. While the underlying, physical mechanisms leading to dispersed growth rates are still debated (cf. Section 3.1), the consequence of GRD for crystallization processes is well-known: an otherwise unexpected broadening of the particle size distribution during growth (Wright and White, 1969; Janse and de Jong, 1976; Tavare, 1985).

PSSD broadening itself is a phenomenon which is frequently observed experimentally,

yet it is often neither modeled quantitatively nor is its exact cause investigated in detail. It is thus likely that in a comparably large number of instances, the effects of growth rate dispersion are falsely attributed to either agglomeration, breakage, spatial variations in the continuous phase within the crystallizer or size dependent growth or vice versa, a fact which has been acknowledged by multiple authors (Garside, 1985; Tavare, 1985; Klug and Pigford, 1989; Ulrich, 1989; Rojkowski, 1993; van Peborgh Gooch et al., 1996; Ma et al., 2002). The role of a correct identification step becomes more apparent given recent efforts in the area of model-based optimization and control of processes (Ma and Wang, 2012; Majumder and Nagy, 2013; Ochsenbein et al., 2013), where model mismatches may lead to unpredicted and undesired behavior of the system when subjected to inputs that have been derived based on an incomplete model.

The overwhelming majority of studies that have investigated GRD in depth have tackled the problem using measurements of facet growth kinetics obtained from a small number of crystals–at a single operating condition–using techniques such as hot stage light microscopy, Michelson interferometry and atomic force microscopy. However, the consequences of the determined extent of GRD for crystal populations are rarely investigated in a quantitative manner. We believe that the combination of different, independent measurement tools, operating at different scales and with different accuracy, presents a promising approach to achieve a quantitative description of GRD at all levels. Hence we propose to couple growth measurements of a number of single crystals (size evolution tracked at a single operating condition) with precise measurements of the instantaneous particle size and shape distributions that stem from desupersaturation experiments carried out in a well-mixed batch crystallizer.

In particular, we aim at re-evaluating measurements obtained previously, in which PSSD broadening had been provisionally accredited to size dependent growth (Ochsenbein et al., 2014), in the light of GRD. The resulting model, a multidimensional (morphological) population balance equation (nD PBE), represents a reconciled and accu-

rate description of the facet growth rate dispersion of β L-glutamic acid (β L-Glu). We emphasize, however, that our intention explicitly is *not* to conclusively determine the physical cause of the observed growth rate dispersion. Rather, we aim at establishing a procedure which uses a more phenomenological (yet quantitative) description of GRD, that remains largely independent of its exact origins, but which eventually may allow to draw some conclusions regarding the possible mechanisms.

This work is organized as follows: first, the methods used to obtain experimental data are described in Section 2. Second, in Section 3, the theoretical basis for growth rate dispersion and its description via population balance models are presented together with an outline of the fitting procedure used in this work. The results of the single crystal experiments, the final fitting and a possible interpretation of the results are given in Section 4. In Section 5 the results of this study are discussed before we present conclusions in Section 6.

2. Materials and Methods

2.1. Materials

L-Glutamic acid monosodium salt hydrate (Sigma Aldrich, Buchs, Switzerland, purity > 99%) and hydrochloric acid (Fluka, Buchs, Switzerland, 37-38%) were used as delivered. Deionized and filtered (filter size 0.22 μm) water was obtained from a MilliQ Advantage A10 system (Millipore, Zug, Switzerland). L-glutamic acid crystallizes in two known polymorphs, i.e., the metastable α and the stable β polymorph, which are monotropically related (Sakata et al., 1961). Seed crystals of the β polymorph were obtained by allowing crystals of the α polymorph to undergo a solution mediated polymorph transformation according to the procedure described in Ochsenbein et al. (2014). β L-Glu crystals grow in a needle shape whose morphology exhibits three facet families, namely {010}, {021}, and {101} (Wang et al., 2007). The unit cell parameters are a = 5.17 Å, b = 17.34 Å, c = 6.95 Å and the space group is $P2_12_12_1$ (Hirokawa, 1955).

2.2. 2D PSSD and Concentration Measurement

The data used in this work is part of that obtained by Ochsenbein et al. (2014). In that work, seeded desupersaturation experiments with varying initial concentrations were performed at constant temperatures in a 2 L temperature controlled stirred tank crystallizer with a stirring rate of 250 rpm. Concentration data was recorded using an ATR-FTIR spectrometer (ReactIR 45m, Mettler Toledo Switzerland) while measurements of the 2D PSSD were obtained using a stereoscopic imaging device, presented elsewhere (Schorsch et al., 2014). For the purpose of this paper we selected four experiments at 25°C with initial supersaturations of 1.10, 1.15, 1.20 and 1.25 and whose experimental durations typically lie in the order of six to ten hours. A short summary of the PSSD reconstruction procedure is provided in the following: the suspension is sampled continuously from the crystallizer and passed through an *ex situ* flow through cell before it is fed back to the system. Particles within the cell are photographed from two orthogonal directions; after a matching and classification step, size and shape are calculated automatically. In the case of β L-glutamic acid, each particle is approximated as a cylinder and characterized by its length, L_1, and width, L_2. The multidimensional particle size distribution is finally reconstructed using all particles measured within the sampling interval (five minutes) via a binning procedure. The resulting distributions are typically based on several tens of thousands of particles each and allow quantitative analysis of the data (Schorsch et al., 2014; Ochsenbein et al., 2014). Note that due to the slow dynamics of the desupersaturation experiments carried out in this work, the time required to obtain a PSSD is negligible.

2.3. Hot Stage Setup

In order to observe the growth of single crystals in a supersaturated solution a temperature controlled measurement cell (diameter: 13 mm, height: 3 mm) made from stainless steel was constructed. The cell and its plastic cover, which prevents evaporation of the solvent, are schematically shown in Figure 1. The lower part of the cell

is comprised of a custom heat sink that is connected to a Peltier element, allowing for rapid and accurate changes of temperature in the measurement cell. The measurement cell is placed under a Zeiss Axioplan microscope that allows for magnifications from 5× to 20× and captures images automatically with a desired frequency. The experimental procedure involves placing a single crystal into the measurement cell, which was filled with saturated solution at a given temperature. The temperature of the solution is then rapidly decreased to the final value, thereby inducing supersaturation and hence crystal growth. An exemplary image of a growing β L-glutamic acid crystal is shown in Figure 2. Analogously to the PSSD measurement, the length L_1 and the width L_2 of the projection are evaluated and their rate of change is used for the determination of growth kinetics. It is worth noting that there is not always a simple one-to-one relationship between the rate of change of L_1 (or L_2) as defined above, and the growth rate of a single crystal facet. Indeed, the measured width of β L-glutamic acid, L_2, depends not only on the rotation of the needle with respect to the camera, but also on the extent to which two independent facets, i.e., {021} and {010}, have grown. Nevertheless, the measured length of a β L-glutamic acid needle can be shown to be a function solely of one facet type, namely the {101} facet (Kitamura and Ishizu, 2000; Ochsenbein et al., 2014). Since the rate of change of L_1, i.e., G_1 and the growth rate in direction of the {101} facet, $G_{\{101\}}$, are proportional, all qualitative statements for the growth rate of measured L_1 are valid also for the true growth rate.

Three additional points are worth making: first, since the solution volume is large compared to the volume of the crystal, the supersaturation remains virtually constant even when the crystal grows (which can be confirmed by a simple mass balance and was verified experimentally). Second, in the light of the extensive literature concerning effects of strain on crystal growth (see Section 3), it was opted not to fix crystals to the measurement cell, as this might introduce additional strain in the crystal, which in turn could affect the growth rate measurements. Third, this design makes the application

of strong convection in the measurement cell impossible, so that our setup is operated under stagnant conditions, as in many other works (Wang and Mersmann, 1992; Jones and Larson, 2000; Virone et al., 2005; Flood, 2010; Dincer et al., 2014; Nguyen et al., 2014). From our previous study on crystals of the β polymorph of L-glutamic acid it is known that growth at low supersaturations is comparably slow (Ochsenbein et al., 2014); an analysis of the characteristic time scales suggests that diffusion is unlikely to limit the crystal growth rate under the given conditions. Furthermore, the crystal growth rates measured for the single crystals compare well with the growth rate estimated from whole crystal populations in a stirred vessel, which further supports this conclusion. A more detailed discussion can be found in Section 5.

3. Theory

3.1. Causes of Growth Rate Dispersion

Janse and de Jong (1976) were probably the first to coin the term "growth rate dispersion" (GRD) to describe the phenomenon of a spread in growth rates for $K_2Cr_2O_7$ crystals; an observation also made prior by Wright and White for sucrose crystals and Natal'ina and Treivus for sucrose and KDP crystals (Wright and White, 1969; Janse and de Jong, 1976; Ulrich, 1989). Soon, it was conjectured that the cause of GRD might be the variation of surface dislocation densities, whose effect on the growth rate is both predicted by Burton-Cabrera-Frank (BCF) theory and confirmed by experimental evidence (cf. Shiau (2003); Dincer et al. (2014) for recent works).

These results notwithstanding, a number of additional factors influencing the growth of crystals have been identified. These include effects caused by lattice strain (Bhat et al., 1987; Ristić et al., 1988; van der Heijden and van der Eerden, 1992; Zacher and Mersmann, 1995; Herden and Lacmann, 1997; Sherwood and Ristić, 2001), or surface roughening (Pantaraks and Flood, 2005; Flood, 2010). These phenomena can cause a fluctuation of the observed growth rate (variability over time) and a growth rate

variance in a population of crystals even when the crystals seem macroscopically identical and the operating conditions (e.g., supersaturation, temperature, etc.) are constant and the same for all crystals. In contrast, Singh and Ramkrishna (2014) explained time-varying growth rates by microscopic supersaturation fluctuations, which, assuming that a crystallizer is well-mixed, cannot explain different growth rates for macroscopically identical crystals.

Given the ongoing debate on the subject, it seems reasonable to assume that growth rate dispersion in general is caused by the interplay of various mechanisms, whose relative importance is likely co-determined by the crystalline system itself, the instantaneous operating conditions and the particle history (Finnie et al., 1999; Jones et al., 2000; Jones and Larson, 2000; Sherwood and Ristić, 2001; Pantaraks and Flood, 2005).

From a descriptive point of view, two models of growth rate dispersion under the conditions typically found in growth experiments (carried out at constant supersaturation and temperature) have emerged: the random fluctuations (RF) and the constant crystal growth (CCG) model. While in the former case, GRD is modeled as temporal variations of the growth rate around a given (but constant) expected value, which gives rise to a second-order dispersive term in the population balance equation, the latter model assumes that crystals are intrinsically born with a distribution of growth rates. While the RF and the CCG models are not mutually exclusive, combined approaches are rare (Zumstein and Rousseau, 1987a,b) and purely CCG-like interpretations are more frequently found in literature. Consequently, a large number of researchers fit standard probability functions, such as normal, log-normal or gamma distributions to time averaged growth rates obtained from single crystal experiments (Garside and Ristić, 1983; Wang and Mersmann, 1992; Zikic et al., 1996; Finnie et al., 1999; Mitrović et al., 2002; Flood, 2010).

In this work, a CCG-like approach is used as well, as it matches the experimental observations presented in Section 4.1; however, the growth rates themselves are not

assumed to be distributed properties as done elsewhere (e.g., by Janse and de Jong (1976); Zumstein and Rousseau (1987a,b)). Rather, a lumped quantity, referred to as *growth affecting property* (*gap*), will be taken as the single factor modifying the growth rates of a crystal (see Section 3.3), an approach that is structurally similar to that of Gerstlauer et al. (2001) (cf. Table 1 for a more detailed comparison). Given the complexity of GRD mechanisms and in the absence of any obvious *a priori* choice for the dominating cause of growth rate dispersion in the β L-glutamic acid system, the introduction of this proxy variable allows for a considerable degree of flexibility while maintaining a manageable level of model complexity.

3.2. Population Balance Modeling

A large number of crystallization processes can be described using the deterministic population balance framework (Hulburt and Katz, 1964; Ramkrishna and Singh, 2014), including those with considerable growth rate dispersion. An overview of a selection of works modeling GRD is given in Table 1. A general formulation for a well-mixed batch system with continuous internal coordinates is given by

$$\frac{\partial}{\partial t} f(t, \mathbf{x}) + \nabla_{\mathbf{x}} \cdot [\mathbf{G}(t, \mathbf{x}, \mathbf{z}) f(t, \mathbf{x})] = B(t, \mathbf{x}, \mathbf{z}) - D(t, \mathbf{x}, \mathbf{z}) \tag{1}$$

where f is the number density function describing the particulate population, which is defined over the set of internal coordinates $\mathbf{x}$, and $\mathbf{G}$ is the velocity field describing the rate of change of internal coordinates, which is usually a function of the state of the continuous phase $\mathbf{z}$ (supersaturation, temperature, pH, etc.) as well. B and D represent "birth" and "death" terms, respectively, allowing for the incorporation of additional mechanisms such as nucleation, agglomeration or breakage of particles. In the case of β L-Glu, whose needle-like crystal shape is approximated by a cylinder with length L_1 and width L_2 and which at the conditions considered does only exhibit growth, Eq. (1) can be recast as

$$\frac{\partial f}{\partial t} + \frac{\partial (G_1 f)}{\partial L_1} + \frac{\partial (G_2 f)}{\partial L_2} + \frac{\partial (G_\mathrm{w} f)}{\partial w} = 0, \tag{2}$$

where we have made use of the surrogate *gap* variable w that was introduced earlier. Note that the applicability of the assumption of absence of nucleation, agglomeration and breakage was verified earlier by Ochsenbein et al. (2014).

While it is clear that the growth rates (in the isothermal case) are generally given as $G_i = G_i(S, \mathbf{L}, w)$ with $i \in \{1, 2\}$, i.e., they are defined as functions of the supersaturation S, the size vector $\mathbf{L}$, and the *growth affecting property* w, their exact functional form is not obvious and depends largely on the nature of w. Similarly, the last term on the l.h.s. of Eq. (2) describes the evolution of the population along the *gap* coordinate; a suitable choice for $G_\mathrm{w} = \mathrm{d}w/\mathrm{d}t$ is also not evident. A set of meaningful options for all convective terms based on fundamental considerations will be presented and discussed in Section 3.3.

Furthermore, the supersaturation in this work is defined as

$$S = \frac{c}{c^*(T)} \tag{3}$$

where c is the solute concentration in the liquid phase and $c^*(T)$ is the solubility and the initial and boundary conditions for the PBE are written as

$$f(0, \mathbf{L}, w) = f_0(\mathbf{L}, w) \tag{4}$$

$$f(t, 0) = 0 \tag{5}$$

where $f_0(\mathbf{L}, w)$ is the size and *gap* distribution of the seed particles, the derivation of which is outlined in Section 3.4. From f, different marginal distributions can be

reconstructed, such as the particle size and shape distribution f_s, which is given by

$$f_\mathrm{s}(t, \mathbf{L}) = \int_0^\infty f(t, \mathbf{L}, w)\, \mathrm{d}w \tag{6}$$

f_s can be measured by imaging devices such as the one presented by Schorsch et al. (2014). To satisfy the conservation of mass, a mass balance equation for the solute concentration in the liquid phase is needed. A general formulation for a closed system is given by

$$\frac{\mathrm{d}c}{\mathrm{d}t} = -\rho_\mathrm{c} \frac{\mathrm{d}}{\mathrm{d}t} \int_C V_\mathrm{c}\left(\mathbf{L}\right) f_\mathrm{s}\left(t, \mathbf{L}\right)\, \mathrm{d}\mathbf{L} \tag{7}$$

where C is the size domain, ρ_c is the density of the crystalline phase and $V_c\left(\mathbf{L}\right)$ is the volume of the crystal with characteristic sizes $\mathbf{L}$. In particular, for the cylindrical particles considered here, $V_\mathrm{c}(L_1, L_2) = \frac{\pi}{4} L_1 L_2^2$, $C = \mathbb{R}^2$, and Eq. (7) can be expressed as:

$$\frac{\mathrm{d}c}{\mathrm{d}t} = -\rho_\mathrm{c} \frac{\pi}{4} \frac{\mathrm{d}\mu_{12}}{\mathrm{d}t} \tag{8}$$

where μ_{12} is a cross-moment of $f_\mathrm{s}(t, L_1, L_2)$, in general defined as

$$\mu_{ij} = \int_0^\infty \int_0^\infty L_1^i L_2^j f_\mathrm{s}(t, L_1, L_2)\, \mathrm{d}L_1 \mathrm{d}L_2 \tag{9}$$

The initial condition for Eq. (7) is:

$$c(0) = c_0 \tag{10}$$

with c_0 being the initial solute concentration.

The three dimensional, first order partial differential equation in Eq. (2), together with the material balance Eq. (8) is solved similar to a standard morphological PBE with three internal coordinates, using a customized finite volume *high resolution* method which solves the corresponding equations for the bounding box containing the distri-

bution (Leveque, 2002; Gunawan et al., 2004; Ochsenbein et al., 2014). This method permits the full reconstruction of the distribution at all times with reasonable computational effort and thus enables a comparison between measured and simulated PSSDs.

3.3. Convective Terms

In the following, a brief discussion of the various convective terms in Eq. (2) is provided. We will begin with an examination of the size growth rates G_1 and G_2 and the possible impact of w on those rates followed by an analysis of G_w.

3.3.1. Size Growth Rates

Under the conditions encountered in this work and up to even higher supersaturations, the growth of β L-Glu was found to be surface integration limited and could be well-described by a "Birth and Spread" type description (Kitamura and Ishizu, 2000; Cornel et al., 2009; Ochsenbein et al., 2014). These results notwithstanding, a useful and flexible empirical relationship for supersaturation dependent growth rates at constant temperature is given by

$$G_i^0(S) = p_{i,1}\,(S-1)^{p_{i,2}} \qquad i \in \{1,2\} \tag{11}$$

where $p_{i,1}$ and $p_{i,2}$ are parameters. The simplest possible approach to incorporate the effect of a *growth affecting property* is by assuming that the growth rates are simply multiplied by some constant, supersaturation and temperature independent factor w

$$G_i(S,w) = w p_{i,1}^0\,(S-1)^{p_{i,2}} \qquad i \in \{1,2\} \tag{12}$$

This result is also obtained when GRD is qualitatively explained through BCF theory, i.e., by variations of the number of co-operating spirals (Garside and Davey, 1980; Klug and Pigford, 1989; Bohlin and Rasmuson, 1992; Shiau, 2003). Note that in Eq. (12), we set $p_{i,1}^0 = 1$ m s^{-1} as w and $p_{i,1}$ cannot be decoupled.

Another common assumption stems from investigations of strain effects, and relates growth rate changes to variations of the chemical potential of the crystals, or in other words, their solubility. The effective solubility thus becomes (Bhat et al., 1987; van der Heijden and van der Eerden, 1992; Gerstlauer et al., 2001; Jones et al., 2000; Virone et al., 2005)

$$c^*_{\mathrm{eff}}(T, w_\mathrm{s}) = c^*(T) \exp\left(\frac{w_\mathrm{s}}{RT}\right) \tag{13}$$

where w_s is the molar strain energy and the growth rate is given accordingly by

$$G_i(S, w_\mathrm{s}) = p_{i,1} \left(S \exp\left(-\frac{w_\mathrm{s}}{RT}\right) - 1\right)^{p_{i,2}} \qquad i \in \{1, 2\} \tag{14}$$

Since we are more interested in the functional form of Eq. (14) than its physical interpretation and as we operate at a single temperature, we will use the substitution $w = w_\mathrm{s}/RT$ in our fittings that employ such a model, i.e., in these cases G_i is written as

$$G_i(S, w) = p_{i,1} \left(S \exp\left(-w\right) - 1\right)^{p_{i,2}} \qquad i \in \{1, 2\} \tag{15}$$

It should be noted that Eq. (15) may result in negative growth rates for crystals exhibiting considerable strain, i.e., if $w_\mathrm{s} > RT \ln(S)$. While the existence of such highly strained crystals cannot be ruled out, we never observed shrinkage (dissolution) of crystals in our experiments. In this work, all growth rates are hence constrained to be non-negative.

An examination of the two models reveals that they predict a different behavior of the growth rate distribution at different supersaturations: Eq. (12) assumes a constant, supersaturation independent distribution of growth rates whereas Eq. (15) implies distributions which are strongly affected by varying supersaturation. Experimental evidence of both behaviors exists, though an increase of growth rate dispersion for increasing

supersaturations is reported more often (Finnie et al., 1999; Jones et al., 2000; Flood, 2010). We will refer to approaches corresponding to Eq. (12) and Eq. (15) as the BCF- and the strain-type of growth, respectively, and will try to fit our data using either option individually. Whereas it is conceivable to apply a growth rate that incorporates both approaches simultaneously (Jones and Larson, 2000), we will assume that the true effect of the *growth affecting property w* is dominated by one type or the other.

We conclude this section with a final remark. There is reason to believe that different facets may be affected differently by the *growth affecting property*, an effect that was also observed experimentally (Sherwood and Ristić, 2001). However, such a situation can only be reliably detected experimentally when the growth rates of various facets are large or the measurement interval is sufficiently long. In order to model growth rate dispersion in a new direction, in principle, either an additional *gap* coordinate needs to be introduced or a (different) relationship between the *growth affecting property* and the new direction needs to be established. In this work, it will be assumed that the effect of the *gap* on the growth rates is either exactly identical for both facets or that *w* does not affect the growth rate in the width direction; all fittings were performed making either assumption.

3.3.2. gap Rate of Change

An important–though often neglected–question in the area of growth rate dispersion is that of whether the growth rate of a single crystal, growing under constant experimental conditions, will remain constant over long time spans (Mitrović et al., 2008, 2009) and related to this, whether or not the growth rate distribution in the reactor is stationary. From a modeling perspective, this determines the nature of the *gap* rate of change, which in our case takes on the unit s^{-1}. Clearly, a physical approach would require a sound understanding of the exact nature of the *growth affecting property* in question. Unfortunately, little is known regarding the evolution of these properties beyond some qualitative speculation.

In many classic CCG approaches, which typically employ a BCF type modification to the growth rates, G_w is assumed to be zero (cf. Table 1). In models employing strain-type growth rates, G_w is often predicted to be negative (strain decreases over time; growth rate increases) and Gerstlauer et al. (2001) give an overview of various possible strain "relaxation" rates based on different assumptions of the absolute lattice strain of crystals and its dependence on the crystal size. In other studies, a temporary decrease of the growth rate after periods of fast growth is reported for crystals subjected to supersaturation swings (Pantaraks and Flood, 2005; Flood, 2010). Table 1 contains information regarding the different assumptions about the rates made in other modeling works. In this work, we will set out to determine whether or not a static *gap* distribution is able to describe the experimental data and, if not, to deduce a number of key characteristics of a non-zero G_w by considering various models for G_w and evaluating their goodness of fit with our experimental data. In this context, we highlight the fact that, in the absence of any experimentally verified and quantitative description of the *gap* rate of change, we utilize a completely empirical expression for G_w.

3.4. Fitting Procedure

A key objective of this work is the quantitative description of growth rate dispersion, both for individual crystal experiments and for experiments with populations of crystals within an agitated batch crystallizer. The demonstration of the feasibility of a simultaneous description is necessary (though not sufficient) to prove the relevance of single crystal data for the behavior of real vessels, yet it is rarely shown (Klug and Pigford, 1989).

Two types of fitting procedures are applied in this work, both of which are designed to solve the problem of the unknown initial distribution of the *growth affecting property* while establishing a connection between single crystal and population data. For both approaches, however, it is assumed that the distribution of growth rates and thus of the *gap* is independent of the initial size and shape of crystals (Zumstein and Rousseau,

1987a), an assumption whose validity will be checked in Section 4.1. The independence assumption implies that

$$f(0, \mathbf{L}, w) = f_{\mathrm{s}}(0, \mathbf{L})\, P_{\mathrm{w}}(0, w) \tag{16}$$

where P_{w} is the *gap* probability density distribution. The two procedures, both visually summarized in form of a flowchart in Figure 3, differ in the way that P_{w} is estimated. In the first case, P_{w} is assumed to be a normal distribution, whose two parameters are fitted along with the remaining growth parameters ('no' case in Figure 3). Clearly, in this way, the observed distribution of growth rates from the single crystal experiments is not necessarily recovered, yet two additional degrees of freedom (mean and variance of the Gaussian) are gained for the fitting. In contrast, in the second approach ('yes' scenario in Figure 3), the single crystal data is fitted well by construction. This is achieved by fitting the parameters of the normal *gap* distribution in a separate step before the actual start of the simulation. In particular, those parameters are found by separately fitting a normal distribution to the dataset $\tilde{\mathbf{w}}$, originating from the single crystal experiments, defined as

$$\tilde{\mathbf{w}} = \begin{bmatrix} \tilde{w}^{(1)} \\ \tilde{w}^{(2)} \\ \vdots \\ \tilde{w}^{(101)} \end{bmatrix} = \begin{bmatrix} g\left(\tilde{G}_1^{(1)}\right) \\ g\left(\tilde{G}_1^{(2)}\right) \\ \vdots \\ g\left(\tilde{G}_1^{(101)}\right) \end{bmatrix} \tag{17}$$

where $\tilde{G}_1^{(i)}$ is the observed growth rate for the i-th single crystal and $g(\cdot)$ is the inverse function of $G_1(S = 1.2, w; \mathbf{p})$ given at $S = 1.20$ (i.e., the supersaturation in those experiments) and the current parameter estimate. Note that the exact $g(\cdot)$ depends on the G_1-function chosen for the fit (either Eq. (12) or Eq. (15)). In the cases in which the inverse element does not exist (Eq. (15) is not bijective), the algorithm chooses the value of w that yields the closest result.

Regardless of the choice of fitting, the population balance model is subsequently solved and its outputs compared to the results of seeded batch desupersaturation experiments, applying the same methods reported in Ochsenbein et al. (2014). In particular, the maximum likelihood estimate is obtained by minimizing the objective function (Bard, 1974)

$$\Phi(\mathbf{p}) = \frac{N_\mathrm{t}}{2} \sum_{i=1}^{N_\mathrm{v}} \ln \left[\sum_{j=1}^{N_\mathrm{t}} \left(y_{ij} - \hat{y}_{ij}(\mathbf{p}) \right)^2 \right] \tag{18}$$

where N_t is the number of observations, N_v is the number of measured outputs, y_{ij} is output i at time j and $\hat{y}_{ij}(\mathbf{p})$ is the corresponding model estimate as a function of the parameters $\mathbf{p}$. The output vector $\mathbf{y}_j$ at time t_j is given by:

$$\mathbf{y}_j = \left[\begin{array}{c} c \\ \overline{L}_1 \\ \sigma_{11} \end{array} \right]_{t=t_j} = \left[\begin{array}{c} c \\ \mu_{10}/\mu_{00} \\ \sqrt{\mu_{20}/\mu_{00} - (\mu_{10}/\mu_{00})^2} \end{array} \right]_{t=t_j} \tag{19}$$

where $\overline{L}_1$ is the mean length of the crystals in the PSSD and σ_{11} represents the standard deviation of the PSSD in L_1 direction.

4. Results

In this section, results of both the single crystal experiments and the fittings of ensemble data in an agitated batch crystallizer using various models are provided. First, the experimental results of the single crystal study are given in Section 4.1. Note that only an analysis of G_1 is provided, as the growth rate in L_2 direction, i.e., the change in the width of the crystals, is excruciatingly slow and therefore hard to quantify. The observed significant dispersion of growth rates in L_1 direction, however, is taken in Section 4.2 as motivation for the use of GRD models in the fitting of ensemble data derived from batch desupersaturation experiments conducted at the same temperature

(Ochsenbein et al., 2014). The findings of the nD PSD data fitting are divided into two parts, representing the different assumptions made.

4.1. Single Crystal Experiments

The evolution of crystal length over time for a number of crystals during the course of single crystal experiments is shown in Figure 4 where the change in time of L_1-size with respect to the initial value is plotted. The growth rate G_1 is initially different for different crystals, exhibiting rather large variability around an average value. As time goes by, growth slows down for all crystals and the variability seems to decrease. While some level of fluctuation of the growth rates lying below the precision of the measurement cannot be ruled out, it is clear that large, time-independent variations exist among the different crystals. Given the line of reasoning in Section 3.4, the properties of the seed crystals at time $t = 0$ are of particular interest; it was therefore decided to utilize only the first 60 minutes of the single crystal experiments, a period in which the growth rate can be reasonably well approximated as constant.

The results of this analysis for 101 particles are visualized in Figure 5, where the scatter plot of G_1 as a function of the initial crystal size together with the corresponding histogram are reported. Visual inspection of the data appears to reveal a lack of size dependence of G_1 with regard to the crystal length, L_1, and only a small effect of the width L_2. A quantitative assessment of potential size dependence can be performed by means of nonlinear regression, in which the data set is fitted to, e.g.

$$G_1 = k_1(1 + L_1)^{k_2} \, (1 + L_2)^{k_3} \tag{20}$$

The result of said fitting is given in Table 2, where the estimated parameter values, the t-statistics and the corresponding p-values are reported. In this table, the p-values for k_2 and k_3 are of interest. The high p-value obtained for k_2 ($p = 0.54$) indicates that the null hypothesis (the data can be explained by a model with $k_2 = 0$; there is no L_1 dependence) cannot be rejected. However, the same statement cannot be made

for L_2: the p-value of parameter k_3 indicates that the null hypothesis can be rejected with high probability and a size dependence of G_1 on L_2 is therefore probable. The magnitude of the estimated size dependence ($k_3 = 0.32$) can be compared to that of the BL2E model presented in Ochsenbein et al. (2014), which was found to be 2.55 ± 0.04. Both the magnitude of the exponent and the sign of the derivative of G_1 with respect to L_2 highlight that the true effect of size on the growth rate is marginal and cannot explain the observed PSSD broadening in itself. Furthermore, given the bigger relative measurement error in the width direction and the still largely unexplained variance in the data (coefficient of determination $r^2 = 0.2$), the assumption that the distribution of growth rates is independent of the size distribution seems to be in fact a reasonable approximation of the initial condition.

We emphasize that the above findings do not necessarily rule out the possibility of having growth rates that are influenced by the initial fragment size of crystals born via secondary nucleation (Wang and Mersmann, 1992; Zekic and Mitrović, 1996), a mechanism potentially important for β L-Glu (Cornel et al., 2009). However, the above results suggest that, for the crystal population present at the beginning of our experiments, i.e., for the seed crystals, this effect would have become negligible.

4.2. Fitting Ensemble Data

The results of fitting the ensemble data with the presented *gap* model and increasingly complex convective terms are reported here. It should be noted that the presented fits can be considered optimal neither in the sense of physical accuracy (as the descriptions of all rates are merely empirical and cannot reasonably cover all possibilities) nor mathematically (since a guarantee of optimality can generally not be provided for these types of systems), therefore we cannot expect to conclusively validate any one model and final parameters should be interpreted as purely empirical. It is worth noting that our optimization routines did repeatedly converge to the same solutions also when started from different initial guesses of the parameters. Regardless, we construct

our argument based on the logic that the minimally complex description that is able to explain the data satisfactorily is likely to possess a set of key features that are present in the real system and we aim at finding such a model.

4.2.1. Static gap Model

As has been pointed out, the presence of a distribution of growth rates (caused by some *gap*) invariably leads to a broadening of the PSSD in the direction of the corresponding characteristic size. Furthermore, the rate of PSSD broadening ($\mathrm{d}\sigma_{11}/\mathrm{d}t$ in the case of the length direction) is higher when the the underlying *gap* distribution is wider. The simplest possible assumption for the *gap* content of crystal is that it remains constant over time, implying a zero rate of change G_w. As pointed out by Gerstlauer et al. (2001), the resulting model is essentially identical to the constant crystal growth model, described for example by Zumstein and Rousseau (1987a,b), yet in our case it is extended to account for particles with two characteristic lengths.

We attempted fitting the morphological PBE model using either BCF- or strain-type growth rates and with or without w dependence of the width growth rate G_2 (i.e., four different combinations). From these static *gap* models, the best BCF-type fit, representative for all results with static *gap*-distributions, was obtained with the following growth rates

$$G_1(S, w) = w p_{i,1}^1 (S-1)^{4.3} \qquad \left[\mathrm{m\ s^{-1}}\right] \tag{21a}$$

$$G_2(S) = 1.3 \times 10^{-2} (S-1)^{10.0} \qquad \left[\mathrm{m\ s^{-1}}\right] \tag{21b}$$

$$G_\mathrm{w} = 0 \qquad \left[\mathrm{s^{-1}}\right] \tag{21c}$$

and the resulting fit is illustrated in Figure 6. Furthermore, in Table 3, we report the mean relative errors (*MRE*) of all quantities, defined for quantity i in a given experiment as

$$MRE_i = \left| \frac{1}{N_\mathrm{t}} \sum_{j=1}^{N_\mathrm{t}} \frac{y_{ij} - \hat{y}_{ij}}{y_{ij}} \right| \tag{22}$$

Clearly, the model is incapable of describing the population data in an adequate manner, whereas the single crystal data is fitted well by construction, cf. Figure 6(a). In fact, a reasonable fit of σ_{11} (third row of Figure 6(b)) must be accompanied by a large increase of the average size of particles, whose magnitude is far greater than that observed experimentally (second row of Figure 6(b)).

Unsurprisingly, the above result can be improved by fitting the initial *gap* distribution using a normal distribution, i.e., by adding two additional parameters to each of the four model variants mentioned above. In that case, the best fit was obtained using a strain-type growth rate in the length direction and no w dependence in the width growth rate; resulting in the following growth rate expressions

$$G_1(S, w) = 6.6 \times 10^{-7} \ (S \exp(-w) - 1)^{1.5} \qquad \left[\mathrm{ms}^{-1}\right] \tag{23a}$$

$$G_2(S) = 4.8 \times 10^{-5} \ (S - 1)^{5.9} \qquad \left[\mathrm{ms}^{-1}\right] \tag{23b}$$

$$G_\mathrm{w} = 0 \qquad \left[\mathrm{s}^{-1}\right] \tag{23c}$$

and a fitted initial *gap* distribution with a mean of 0.22 and standard deviation of 0.07. Such a model allows to reduce the objective function value significantly, as can also be seen from the overall much better fit in Figure 7(b) and the corresponding entry in Table 3. However, this appreciable improvement in the description of the population data requires a large modification of the initial *gap* distribution, resulting in a growth rate distribution that is entirely inconsistent with the data obtained from the single crystal experiments (cf. Figure 7(a)). In particular, in order to describe the PSSD data, from a modeling point of view, a strong increase of the *gap* distribution variance is required. This implies the existence a large number of particles whose growth is completely arrested from the beginning of each experiment, an effect that reduces the increase in

average size $\overline{L}_1$ necessary to achieve a given gain in σ_{11}.

Summarizing, it was found that describing the two data sets in any satisfactory manner when using a *gap* rate of change of zero ($G_w = 0$) is impossible. While an accurate description of only the PSSD data alone is feasible, this requires the conjuring of a large number of non-growing crystals in the model. Such crystals were however not observed in the single crystal experiments. Moreover, any static model will predict a constant growth rate for each crystal, which markedly contradicts the time resolved ΔL_1 vs. t curves obtained from the single crystal experiments (cf. Figure 4).

4.2.2. Dynamic gap Model

As discussed in Section 3.3.2, considering the possible physical causes that motivated the introduction of the *growth affecting property* variable w in Section 3.1 it is not unreasonable to assume that the absolute or relative content of the intrinsic property might be subject to changes over time, i.e., that $G_\mathrm{w} \neq 0$. The single crystal experiments results (cf. Figure 4), too, seem to indicate a change of the growth rate over time. While the information of the change in G_1 contained in these experiments could not be utilized in a quantitative manner (see Section 5.1 for details), these experiments allow us to surmise two important qualities of the dynamic behavior of the GRD. First, it allows us to infer the sign of G_w (namely, G_w is negative when using a BCF-type modification of G_i and positive in the strain-type case; the rate of growth slows down). Second, it can be seen that the variance of the G_1 (and hence also the *gap*) distribution decreases with time, which remains true regardless of the growth rate modification used.

The latter observation is of particular importance given the results with the static *gap* model in Section 4.2.1, where it evident that the quality of fit for the batch data improves with increasingly broad (static) *gap* distributions, yet that such distributions differ significantly from the experimentally observed ones. Clearly, a mere decrease of the growth rate–when applied to all crystal sizes uniformly– is therefore also not able to describe the batch experiments.

In order to reconcile the above considerations, we propose the presence of a selective driving force that makes a certain type of crystals change their growth rate faster or slower than others. One of the ways to achieve a significant increase in the width of the PSSD in L_1 direction, σ_{11}, early on, is to make this driving force depend on the size of the crystal. We therefore suggest the following empirical expression for the *gap* rate of change, G_w

$$G_\mathrm{w} = p_{\mathrm{w},1}\, L_1^{p_{\mathrm{w},2}} G_1^{p_{\mathrm{w},3}} \tag{24}$$

From the above mentioned models (employing the four different combinations of growth rates) with this dynamic *gap* rate of change the following model yielded the best fit we could identify

$$G_1(S, w) = 2.0 \times 10^{-6} \left(S \exp\left(-w\right) - 1\right)^{2.2} \qquad \left[\mathrm{m\ s^{-1}}\right] \tag{25a}$$

$$G_2(S, w) = 3.6 \times 10^{-4} \left(S \exp\left(-w\right) - 1\right)^{4.5} \qquad \left[\mathrm{m\ s^{-1}}\right] \tag{25b}$$

$$G_\mathrm{w} = 36.8\, L_1^{-2.0} G_1^{1.2} \qquad \left[\mathrm{s^{-1}}\right] \tag{25c}$$

The fitting results are illustrated in Figure 8 and Table 3, where a clear improvement of the quality of fit is visible. Nevertheless, there still exists a non-negligible discrepancy between experimental results and model output, which might be caused by a (still) too simplistic model of G_w. Moreover, while multiple initial points were evaluated in the parameter space and different optimization algorithms were used, the identification of global optima is a difficult endeavor for these complex models.

In addition to showing fitting outputs, analyses of the different marginal distributions are possible. In Figure 9, various volume weighted, marginal distributions, (defined in a similar manner as the size and shape distribution in Eq. (6)) for one experiment ($S_0 = 1.20$) in the beginning and end are shown; in the case of the PSSD, the model output is compared with the experimentally measured distributions. Focusing first on the

final PSSD (Figure 9(d)), one can see that the variance of the model output is slightly too low, but that the overall movement of the PSSD is generally well captured. As shown in the remaining marginal distributions, i.e. figures c) to f), there is a significant torsion of the distribution. In the end of the process, larger crystals generally possess a smaller *gap* content due to the fact that a) crystals with low *gap* content grow faster (in the case of strain-type growth) and b) smaller crystals have a faster build-up of *gap* (cf. Eq. (25c)). Furthermore, in Figure 10, the initial/final *gap* and growth rate distribution for the same operating conditions are shown, thus indicating that the growth rate distribution is indeed expected to decrease both in mean and variance over the course of the process, a behavior not unlike that exhibited in the single crystal experiments (cf. Figure 4).

In addition, we have tested the predictive capabilities of the dynamic *gap* model by means of two types of comparisons, the results for which we report in Table 3. First, the ability to interpolate was verified by fitting three out of the four experiments at $T = 25°C$ and predicting a fourth, whose initial supersaturation lies in between the others. Second, we have compared the model prediction with the parameters in Eq. (25) to an additional experiment performed in our initial study, conducted at a higher temperature (30°C) and with a supersaturation of 1.18 (labeled VER1 in (Ochsenbein et al., 2014)), i.e., in this case we use the model to extrapolate in terms of temperature. In both cases, the predictive capabilities of the model are satisfactory, as indicated by the small mean relative errors in Table 3, with a clear decrease in accuracy for the latter case, in which the model is extrapolated.

In order to arrive at a definitive picture of the physical mechanism(s) underlying growth rate dispersion, a substantially extended experimental data set, consisting of experiments conducted in realistic batch conditions as well as experiments probing the fundamental origin of the growth affecting property would be required (see also the discussion in Section 5). Nevertheless, a *preliminary* interpretation, consistent with the

experimental evidence as well as with the proof-of-concept fitting results provided in this article, shall be given. A valid hypothesis might be that the surface of the seed crystals is initially rough, i.e., riddled with kink sites, leading to an acceleration of growth in the early stages. With time, the particles might slowly undergo a healing or refacetting step, whose duration and extent might be affected by the crystal size (e.g., via the total crystal surface area).

5. Discussion

5.1. Single Crystal Data

As one of the major goals of the current work is to establish a quantitative connection between shape measurements conducted at the single particle and at the population level, a discussion of the suitability of the used hot stage setup and the corresponding single crystal data is essential. It is clear that, for any comparison to be meaningful, the growth conditions in the lab-scale reactor and the hot stage should be comparable. It is well-known that impurities in the crystals or in the solution could change the growth rate (Sangwal, 2007; Vetter, 2012). However, all solutions and seed crystals used in this work stem from the same batch of L-glutamic acid (which was also used to generate the population data reported in Ochsenbein et al. (2014)) and have been carried out using highly pure water as solvent. Therefore, the GRD observed in our experiments cannot simply be explained by varying impurity profiles between different experiments. However, we can immediately identify two important aspects that are absent in the hot stage: stirring and particle collisions. Concerning the first point, it has already been pointed out that the growth of β L-glutamic acid is slow enough to be surface-integration controlled even in the absence of stirring. Regarding the missing particle-particle (or particle-impeller/particle-wall) interactions: the growth rate distribution might well be affected by collisions, e.g., by causing imperfections in the growing crystal surfaces. It seems reasonable to assume that collisions, due to their in-

herently stochastic nature, would therefore intensify an inherently present growth rate distribution. However, by additionally trying to fit the *gap* distribution in Section 4.2.1, we have implicitly accounted for the possibility of a broader distribution. Regardless, we believe that solely relying on single crystal experiments to characterize the extent of GRD in an industrial crystallization process is not advisable.

Finally, we would like to comment on the possibility of extracting information regarding G_{w} (and its potential size dependence) from single crystal data. While potentially feasible, a quantitative analysis would require a large number ($\gg$100) of sampled crystals, whose initial size and shape should ideally be controlled, a feat that is difficult to achieve. While such measurements would be of great interest, we regard them as beyond the scope of the current work.

5.2. Modeling and Fitting

The modeling and fitting procedures presented here are the key tools allowing for a better interpretation of the experimental data. It is therefore important to clearly outline the possible applications together with the limitations of the described morphological population balance equations.

We emphasize the fact that an important assumption made is that of a size independent, initial growth rate distribution. While the experimental evidence reported in Section 4.1 suggests that this approximation is a meaningful one, it is worthwhile to discuss the potential ramifications of it being incorrect. Essentially, the necessity for G_{w} to be a function of size diminishes with increasing violation of the above assumption. Hence, without a more detailed analysis of the size dependence of the growth rate dispersion of the seed crystals, involving again the measurement of many more particles, we cannot necessarily rule out the possibility that the proposed size dependence of G_{w} is an artifact of some underlying effects and care should be taken not to over-interpret the results. Nonetheless, it should be noted that the dynamic *gap* model presented in Section 4.2.2 neither represents just an increase in the number of parameters in order to

fit more data better, nor does it serve as a simple shift of the size dependence from the growth rate G_1 to some other convective term. The lack of a strong size dependence of the growth rate together with the large observed scatter does *necessitate* the use of (at least) one additional internal coordinate to achieve a more physically correct model. The size and shape of crystals or the properties of the continuous phase, which are the only physical variables in the classic population balance model without growth rate dispersion, are demonstrably insufficient to explain both types of experimental observations reported here. Furthermore, the fact that a size dependent growth model is able to fit the data (as demonstrated in Ochsenbein et al. (2014)) is a consequence of G_w (or the initial growth rate distribution) being a function of size, not the other way around.

Concerning the numerical complexity, the relatively high dimensionality of the *gap* model together with the strongly varying convective terms make it barely suited for use within an optimization routine. It is also for this reason that the achieved fits can at best be described as a proof-of-concept. We thus do not recommend the use of such models for the design or optimization of real processes, particularly given the unknown physical nature of both w and G_w.

5.3. Scientific and Industrial Relevance

Regarding the scientific and industrial value of this work, first and foremost, we highlight the fact that the current study is indeed one of seed crystals and their properties, i.e., crystals which enter the process with a history. Studies of seed materials are highly relevant, since the overwhelming majority of industrial processes carried out in batch crystallizers are seeded; however little is known regarding the systematic and mechanistically informed preparation of such particles.

Additionally, this work concerns itself with the evolution of GRD over time. As such, it lays the basis for a better understanding of how growth kinetics are affected by process conditions. Note that these effects might be either unintentional, as in the case of needle breakage, or deliberate. Clearly, gaining insight in what causes GRD and how

to reproduce it-or even minimize it–could be of considerable value in this context.

6. Conclusion and Outlook

The growth rate dispersion of β L-glutamic acid needles in the length direction was investigated by means of two independent imaging methods, one dedicated to the measurement of the instantaneous particle size and shape distribution in the crystallizer over time, the other to the tracking of the particle morphology for individual crystals. After deducing the presence of a *growth affecting property (gap)* in the crystals from single crystal data, the population balance framework was used to design a description of the system, the *gap* model, that allows combining the complementary information contained in both data sets through the initial condition. It was further shown that the *gap* content in the particles is subject to change over time. Finally, through a proof-of-concept fitting procedure, the hypothesis that the rate of change is influenced by particle size was formulated and found to yield a plausible explanation for the experimentally observed phenomena. However, in order to conclusively rule out other possibilities, further experimental data would be required, as we have highlighted throughout this article.

We perceive the value of this study to be two-fold: first, it highlights the added benefit that results from using multi-scale approaches that employ a combination of independent measurement techniques to the study of crystallization phenomena, since individual tools may not offer full insight into the different aspects affecting the process. While this work focuses on crystal growth, we believe this to be true also in the case of nucleation, agglomeration, etc. Second, the present work showcases the potential benefits of using quantitative analysis of experimental data sets through process models. While the resulting mathematical description may not necessarily be practical as a design tool for process optimization, it represents a more comprehensive and physically sound view of the observed phenomena, thus allowing for a deeper understanding

of the process. The resulting qualitative lessons could then be used to guide process development as well as to identify further research directions in order to establish a more complete picture of crystallization.

Acknowledgements

The authors are thankful to the Swiss National Science Foundation for their support (project number 200021-155971).

Notation

B	birth term in the PBE	[m^{-2} kg^{-1} s^{-1}]
C	space domain	[-]
c	solute concentration in the liquid phase	[kg kg^{-1}]
c_0	initial solute concentration in the liquid phase	[kg kg^{-1}]
c^*	solubility	[kg kg^{-1}]
c^*_{eff}	effective solubility	[kg kg^{-1}]
D	death term in the PBE	[m^{-2} kg^{-1} s^{-1}]
f	number density function	[m^{-n} kg^{-1}]
f_{s}	marginal shape distribution	[m^{-n} kg^{-1}]
f_0	PSD of seed crystals	[m^{-n} kg^{-1}]
$\mathbf{G}$	vector of rates of change	[varies]
$\hat{G}_1^{(i)}$	observed length growth rate of i'th crystal in single crystal experiments	[m s^{-1}]
g	inverse of G_1 at given S and $\mathbf{p}$	[-]
$\mathbf{k}$	vector of growth rate parameters	[varies]
$\mathbf{L}$	vector of characteristic lengths	[m]
MRE_i	mean relative error of i'th quantity	[-]
N_t	number of observations	[-]
N_v	number of measured outputs	[-]
P_{w}	*gap*-distribution	[-]
$\mathbf{p}$	vector of growth rate parameters	[varies]
R	gas constant	[J mol^{-1} K^{-1}]
S	supersaturation	[-]
S_0	peak supersaturation	[-]
T	temperature	[K]
t	time	[s]
V_{c}	single crystal volume	[m^3]
w	growth affecting property	[-]
$\hat{\mathbf{w}}$	*gap* dataset	[-]
w_{s}	molar strain energy	[J mol^{-1}]
$\mathbf{x}$	state vector of particle properties	[varies]
y_{ij}	output i at time j	[varies]
$\mathbf{z}$	state vector of continuous phase	[varies]

Greek letters

μ_{ij}	ij-cross moment of shape distribution	[m^{i+j} kg^{-1}]
ρ_{c}	crystal density	[kg m^{-3}]
σ_{11}	standard deviation of shape distribution in L_1 direction	[m]
Φ	objective function for parameter estimation	[-]

References

Bard, Y., 1974. Nonlinear Parameter Estimation. Academic Press.

Bhat, H. L., Sherwood, J. N., Shripathi, T., 1987. The influence of stress, strain and fracture of crystals on the crystal growth process. Chem. Eng. Sci. 42, 609–618.

Bohlin, M., Rasmuson, Å. C., 1992. Modeling of Growth Rate Dispersion in Batch Cooling Crystallization. AIChE J. 38, 1853–1863.

Borchert, C., Temmel, E., Eisenschmidt, H., Lorenz, H., Seidel-Morgenstern, A., Sundmacher, K., 2014. Image-Based in Situ Identification of Face Specific Crystal Growth Rates from Crystal Populations. Cryst. Growth Des. 14 (3), 952–971.

Cornel, J., Lindenberg, C., Mazzotti, M., 2009. Experimental Characterization and Population Balance Modeling of the Polymorph Transformation of L -Glutamic Acid. Cryst. Growth. Des. 9, 243–252.

Dincer, T. D., Ogden, M. I., Parkinson, G. M., 2014. Investigation of growth rate dispersion in lactose crystallisation by AFM. J. Cryst. Growth 402, 215–221.

Finnie, S. D., Ristić, R. I., Sherwood, J. N., Zikic, A. M., 1999. Morphological and growth rate distributions of small self-nucleated paracetamol crystals grown from pure aqueous solutions. J. Cryst. Growth 207, 308–318.

Flood, A. E., 2010. Feedback between crystal growth rates and surface roughness. CrystEngComm 12, 313–323.

Garside, J., 1985. Industrial Crystallization from Solution. Chem. Eng. Sci. 40, 3–26.

Garside, J., Davey, R. J., 1980. Secondary Contact Nucleation: Kinetics, Growth and Scale-up. Chem. Eng. Commun. 4, 393–424.

Garside, J., Ristić, R. I., 1983. Growth Rate Dispersion among ADP Crystals formed by Primary Nucleation. J. Cryst. Growth 61, 215–220.

Gerstlauer, A., Mitrović, A., Motz, S., Gilles, E.-D., 2001. A population model for crystallization processes using two independent particle propertiess. Chem. Eng. Sci. 56, 2553–2565.

Gunawan, R., Fusman, I., Braatz, R. D., 2004. High resolution algorithms for multidimensional population balance equations. AIChE J. 50, 2738–2749.

Herden, A., Lacmann, R., 1997. The crystallization of potassium nitrate II. Growth rate dispersion. J. Cryst. Growth 179, 592–604.

Hirokawa, S., Oct. 1955. A new modification of L-glutamic acid and its crystal structure. Acta Crystallographica 8 (10), 637–641.

Hulburt, H. M., Katz, S., 1964. Some problems in particle technology. Chem. Eng. Sci. 19, 555–574.

Janse, A. H., de Jong, E. J., 1976. The occurence of growth dispersion and its consequences. In: Mullin, J. W. (Ed.), Industrial Crystallization. Springer, pp. 145–154.

Jones, C. M., Larson, M. A., 2000. Using dislocations and integral strain to model the growth rates of secondary nuclei. Chem. Eng. Sci. 55, 2563–2570.

Jones, C. M., Larson, M. A., Ristić, R. I., Sherwood, J. N., 2000. The role of dislocations, integral strain, and supersaturation on the growth rates of sodium nitrate. J. Cryst. Growth 208, 520–524.

Kitamura, M., Ishizu, T., 2000. Growth kinetics and morphological change of polymorphs of L-glutamic acid. J. Cryst. Growth 209, 138–145.

Klug, D. L., Pigford, R. L., 1989. The Probability Distribution of Growth Rates of Anhydrous Sodium Sulfate Crystals. Ind. Eng. Chem. Res. 28, 1718–1725.

Leveque, R., 2002. Finite-volume methods for hyperbolic problems. Cambridge University Press.

Ma, C. Y., Wang, X. Z., 2008. Crystal Growth Rate Dispersion Modeling Using Morphological Population Balance. AIChE J. 54, 2321–2334.

Ma, C. Y., Wang, X. Z., 2012. Model identification of crystal facet growth kinetics in morphological population balance modeling of L -glutamic acid crystallization and experimental validation. Chem. Eng. Sci. 70, 22–30.

Ma, D. L., Braatz, R. D., Tafti, D. K., 2002. Compartmental Modeling of Multidimensional Crystallization. Int. J. Mod. Phys. B 16, 383–390.

Majumder, A., Nagy, Z., 2013. Prediction and control of crystal shape distribution in the presence of crystal growth modifiers. Chem. Eng. Sci. 101, 593–602.

Mitrović, M., Žekic, A., Ilic, Z., 2002. Connection between the growth rate distribution and the size dependent crystal growth. Chem. Phys. Let. 361, 312–316.

Mitrović, M. M., Žekić, A. A., Baros, Z. Z., 2008. Growth rate changes of sodium chlorate crystals independent of growth conditions. Chem. Phys. Lett. 464, 38–41.

Mitrović, M. M., Žekić, A. A., Baros, Z. Z., 2009. Stability of growth rate of sodium chlorate. Chem. Phys. Lett. 467, 299–303.

Nguyen, T. T. H., Hammond, R. B., Roberts, K. J., Marziano, I., Nichols, G., 2014. Precision measurement of the growth rate and mechanism of ibuprofen {001} and{011} as a function of crystallization environment. CrystEngComm 16, 4568–4586.

Ochsenbein, D. R., Schorsch, S., Vetter, T., Mazzotti, M., Morari, M., September 2013. Closed-loop control of a crystallization process using morphology measurements. In: Proceedings of the 20th international Workshop on Industrial Crystallization (BIWIC). pp. 115–122.

739 Ochsenbein, D. R., Schorsch, S., Vetter, T., Mazzotti, M., Morari, M., 2014. Growth
740 Rate Estimation of β L-Glutamic Acid from Online Measurements of Multidimen-
741 sional Particle Size Distributions and Concentration. Ind. Eng. Chem. Res. 53, 9136–
742 9148.

743 Pantaraks, P., Flood, A. E., 2005. Effect of Growth Rate History on Current Crystal
744 Growth: A Second Look at Surface Effects on Crystal Growth Rates. Cryst. Growth
745 Des. 5, 365–371.

746 Ramkrishna, D., Singh, M. R., 2014. Population Balance Modeling: Current Status
747 and Future Prospects. Annu. Rev. Chem. Biomol. Eng. 5, 123–146.

748 Ristić, R. I., Sherwood, J. N., Wojciechowski, K., 1988. Assessment of the strain in
749 small sodium chlorate crystals and its relation to growth rate dispersion. J. Cryst.
750 Growth 91, 163–168.

751 Rojkowski, Z., 1993. Crystal Growth Rate Models and Similarity of Population Bal-
752 ances for Size-Dependent Growth Rate and for Constant Growth Rate Dispersion.
753 Chem. Eng. Sci. 48, 1475–1485.

754 Sakata, Y., Horikawa, T., Takenouchi, K., 1961. Studies on the Behaviors of Impurities
755 on the Crystallization of L-glutamic Acid. I. Behavior of amino acids and inorganic
756 salts. Agr. Biol. Chem. Tokyo 25, 921–925.

757 Sangwal, K., 2007. Additives and Crystallization Processes: From Fundamentals to
758 Applications. John Wiley & Sons.

759 Schorsch, S., 2014. Imaging Systems, Analysis Protocols, and Modelling Tools for
760 Particle Shape Monitoring for Crystallization. Ph.D. thesis, ETH Zürich.

761 Schorsch, S., Ochsenbein, D., Vetter, T., Morari, M., Mazzotti, M., 2014. High ac-
762 curacy online measurement of multidimensional particle size distributions during
763 crystallization. Chem. Eng. Sci. 105, 155–168.

764 Schorsch, S., Vetter, T., Mazzotti, M., 2012. Measuring multidimensional particle size
765 distributions during crystallization. Chem. Eng. Sci. 77, 130–142.

766 Sherwood, J. N., Ristić, R. I., 2001. The influence of mechanical stress on the growth
767 and dissolution of crystals. Chem. Eng. Sci. 56, 2267–2280.

768 Shiau, L.-D., 2003. The distribution of dislocation activities among crystals in sucrose
769 crystallization. Chem. Eng. Sci. 58, 5299–5304.

770 Singh, M. R., Ramkrishna, D., 2013. A Comprehensive Approach to Predicting Crystal
771 Morphology Distributions with Population Balances. Cryst. Growth Des. 13, 1397–
772 1411.

773 Singh, M. R., Ramkrishna, D., 2014. Dispersions in crystal nucleation and growth
774 rates: Implications of fluctuation in supersaturation. Chem. Eng. Sci. 107, 102–113.

775 Tavare, N. S., 1985. Crystal Growth Rate Dispersion. Can. J. Chem. Eng. 63, 436–442.

Ulrich, J., 1989. Growth Rate Dispersion - A Review. Cryst. Res. Tech. 24, 249–257.

van der Heijden, A. E. D. M., van der Eerden, J. P., 1992. Growth rate dispersion: the role of lattice strain. J. Cryst. Growth 118, 14–26.

van Peborgh Gooch, J. R., Hounslow, M. J., Mydlarz, J., 1996. Discriminating between size-enlargement mechanisms. Chem. Eng. Res. Des. 74, 803–811.

Vetter, T., 2012. Optimizing The Crystallization Of Pharmaceutical Compounds Using Additives. Ph.D. thesis, ETH Zürich.

Virone, C., ter Horst, J. H., Kramer, H. J. M., Jansens, P. J., 2005. Growth rate dispersion of ammonium sulphate attrition fragments. J. Cryst. Growth 275, e1397–e1401.

Wang, S., Mersmann, A., 1992. Initial-size-dependent growth rate dispersion of attrition fragments and secondary nuclei. Chem. Eng. Sci. 47, 1365–1371.

Wang, X., Roberts, K., Ma, C., 2008. Crystal growth measurement using 2D and 3D imaging and the perspectives for shape control. Chem. Eng. Sci. 63, 1173–1184.

Wang, X. Z., Calderon de Anda, J., Roberts, K., 2007. Real-time measurement of the growth rates of individual crystal facets using imaging and image analysis - A feasibility study on needle-shaped crystals of L-glutamic acid. Chem. Eng. Res. Des. 85, 921–927.

Wright, P. G., White, E. T., 1969. Size Distribution Studies in Sugar Crystallization. In: Proc. Qd. Soc. Sugar Cane Technol. pp. 299–309.

Zacher, U., Mersmann, A., 1995. The influence of internal crystal perfection on growth rate dispersion in a continuous suspension crystallizer. J. Cryst. Growth 147, 172–180.

Zekic, A. A., Mitrović, M. M., 1996. Improvement of Initial Conditions of the Crystal Growth by Dissolution and Refaceting. Cryst. Res. Technol. 158, 560–567.

Zikic, A. M., Ristić, R. I., Sherwood, J. N., 1996. Three-parameter distribution function fit to growth rate dispersion among small crystals. J. Cryst. Growth 158, 560–567.

Zumstein, R. C., Rousseau, R. W., 1987a. Growth rate dispersion by initial growth rate distributions and growth rate fluctuations. AIChE J. 33, 121–129.

Zumstein, R. C., Rousseau, R. W., 1987b. Growth Rate Dispersion in Batch Crystallization with transient conditions. AIChE J. 33, 1921–1925.

Table 1: Overview of Growth Rate Dispersion Modeling Works. L refers to a characteristic size while w represents a GRD related property.

Reference	**Internal PBE coordinates**	**Growth Rate**	**G_w**	**Remarks**
This work	L_1, L_2, w	BCF or strain	non-zero	
Gerstlauer et al. (2001)	L, w	strain	non-zero	
Ma and Wang (2008)	L_1, L_2, L_3	strain	n/a	w not an independent property, but explicit function of $\mathbf{L}$
Bohlin and Rasmuson (1992)	L, w	BCF	zero	
Klug and Pigford (1989)	L, w	BCF	zero	
Zumstein and Rousseau (1987a,b)	L, w	BCF	zero	Combined CCG + RF model
Jones and Larson (2000)	n/a	BCF and Strain	n/a	
Shiau (2003)	n/a	BCF	n/a	

Table 2: Nonlinear regression results of G_1 data

	Estimate	**st. dev.**	**t-statistic**	**p-value**
k_1	3.00E-03	1.00E-03	2.41	0.02
k_2	0.04	0.06	0.61	0.54
k_3	0.32	0.07	4.38	3.00E-03

Table 3: Mean relative errors (MREs) of PSSD data for different fittings and predictions

Description	S_0 [-]	T [°C]	MRE_{conc} [%]	MRE_{length} [%]	MRE_{stddev} [%]
Static *gap* model fit	1.10	25	0.3	2.7	7.1
	1.15	25	0.2	20.9	0.7
	1.20	25	0.4	71.0	3.3
	1.25	25	1.5	71.5	1.4
Static *gap* model fit (additional fitting of measured G_1 data)	1.10	25	0.4	1.1	7.1
	1.15	25	0.5	1.7	1.4
	1.20	25	0.1	0.4	1.6
	1.25	25	0.6	0.2	1.4
Dynamic *gap* model fit	1.10	25	0.4	1.0	7.3
	1.15	25	0.5	0.5	4.3
	1.20	25	0.2	1.2	0.02
	1.25	25	0.01	1.0	2.3
Predict experiment with $S_0 = 1.15$, fit remaining	1.15	25	0.2	1.7	4.8
Predict experiment with $S_0 = 1.20$, fit remaining	1.20	25	0.04	2.4	1.6
Predict experiment at $T = 30$°C with fit at $T = 25$°C	1.18	30	1.8	0.2	7.7

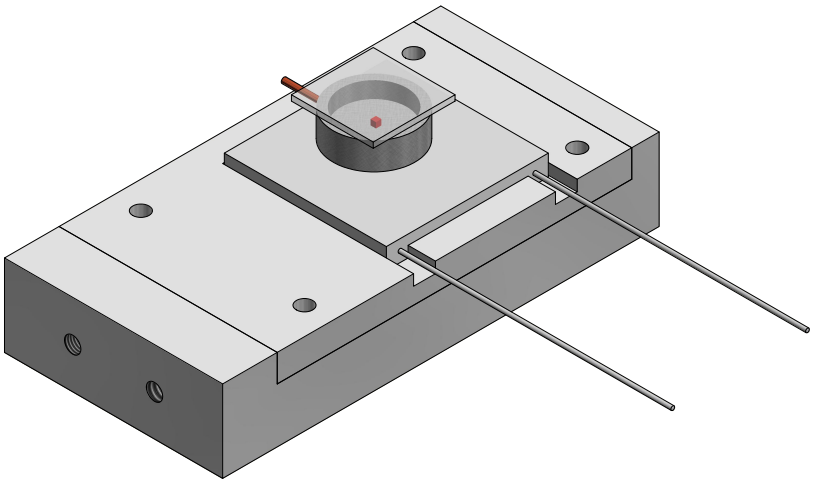

Figure 1: Schematic of the Hot Stage Setup.

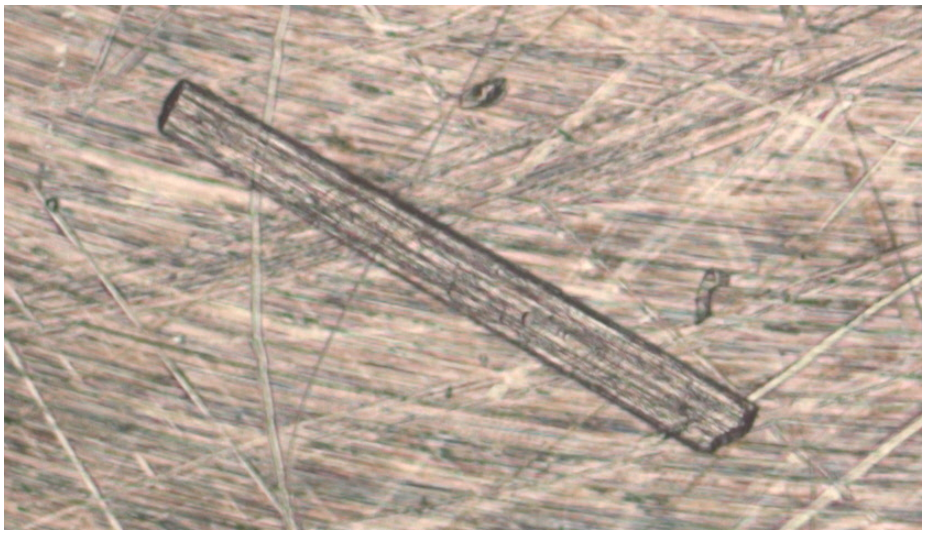

Figure 2: Example image of a β L-glutamic acid crystal in the hot stage.

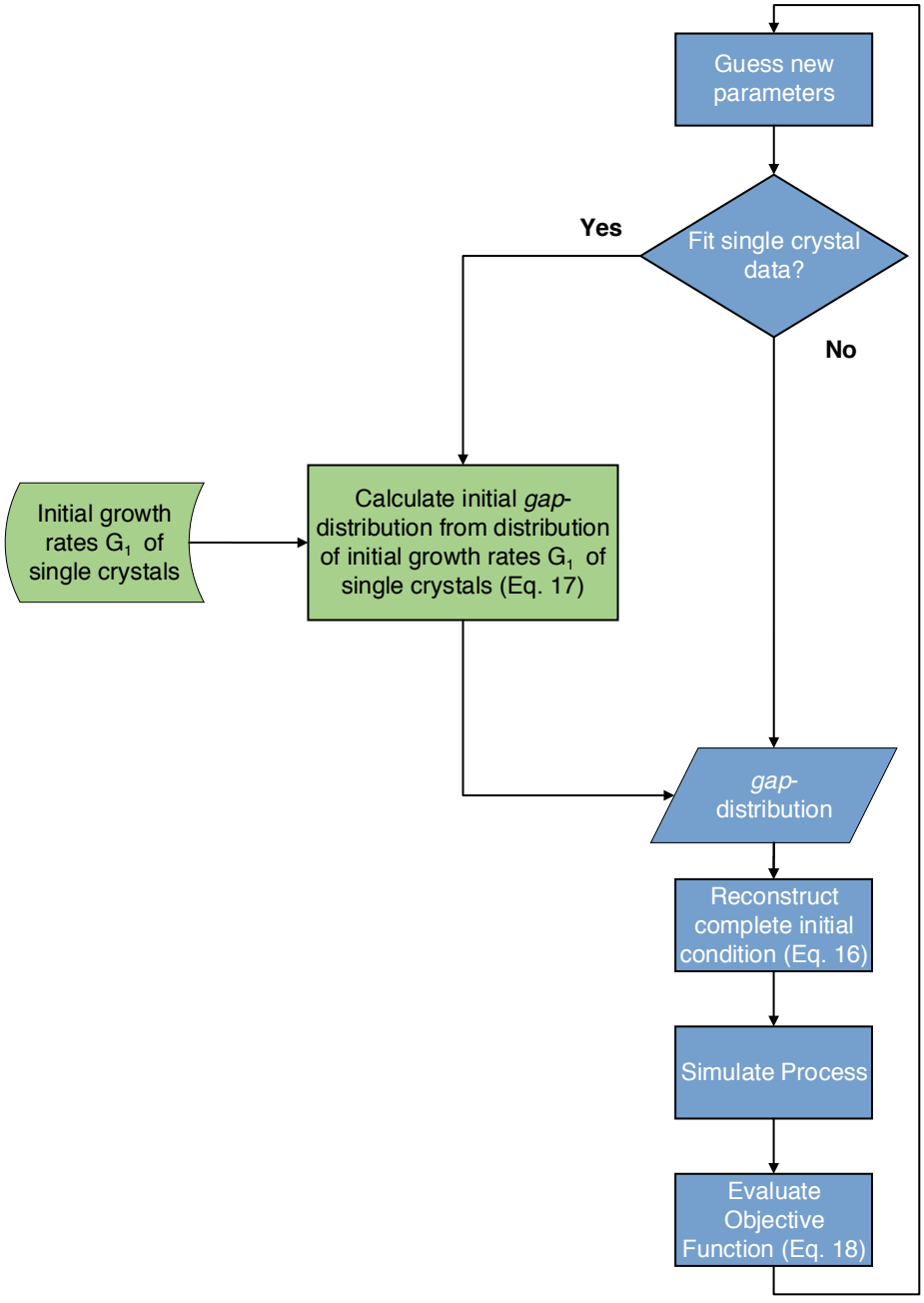

Figure 3: Schematic of the fitting procedure.

.

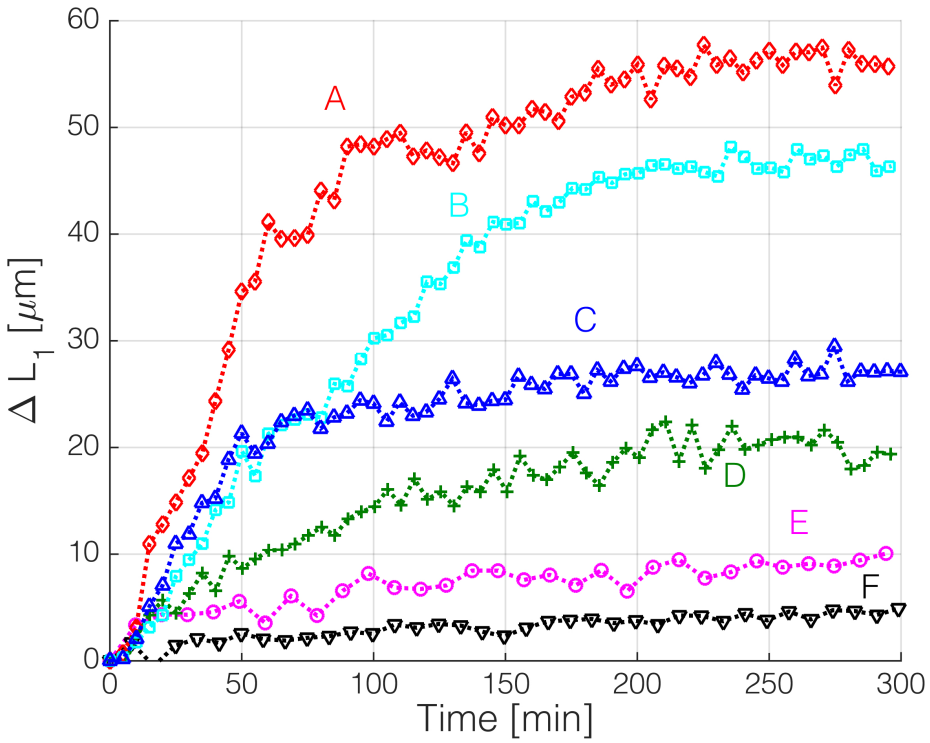

Figure 4: ΔL_1 vs. time curve for different crystals. Individual measurement points are given by the mean of three size evaluations. Initial size vectors for the crystals: $\mathbf{L}^{\mathrm{A}} = [505,\ 59]^\intercal$ µm, $\mathbf{L}^{\mathrm{B}} = [442,\ 38]^\intercal$ µm, $\mathbf{L}^{\mathrm{C}} = [261,\ 46]^\intercal$ µm, $\mathbf{L}^{\mathrm{D}} = [152,\ 45]^\intercal$ µm, $\mathbf{L}^{\mathrm{E}} = [228,\ 34]^\intercal$ µm, $\mathbf{L}^{\mathrm{F}} = [177,\ 33]^\intercal$ µm.

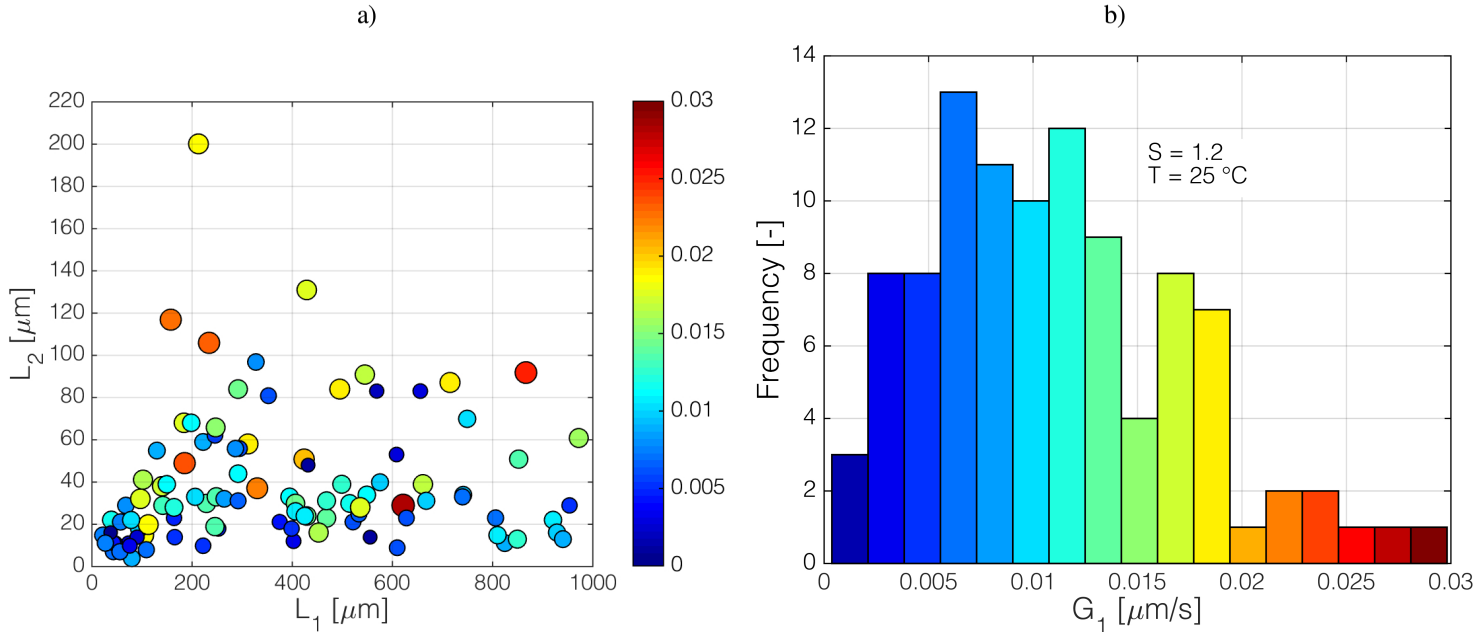

Figure 5: (a) Scatter plot of growth rates G_1 as function of initial crystal size and (b) histogram of growth rates. Size and color of markers in (a) indicate the magnitude of the growth rate.

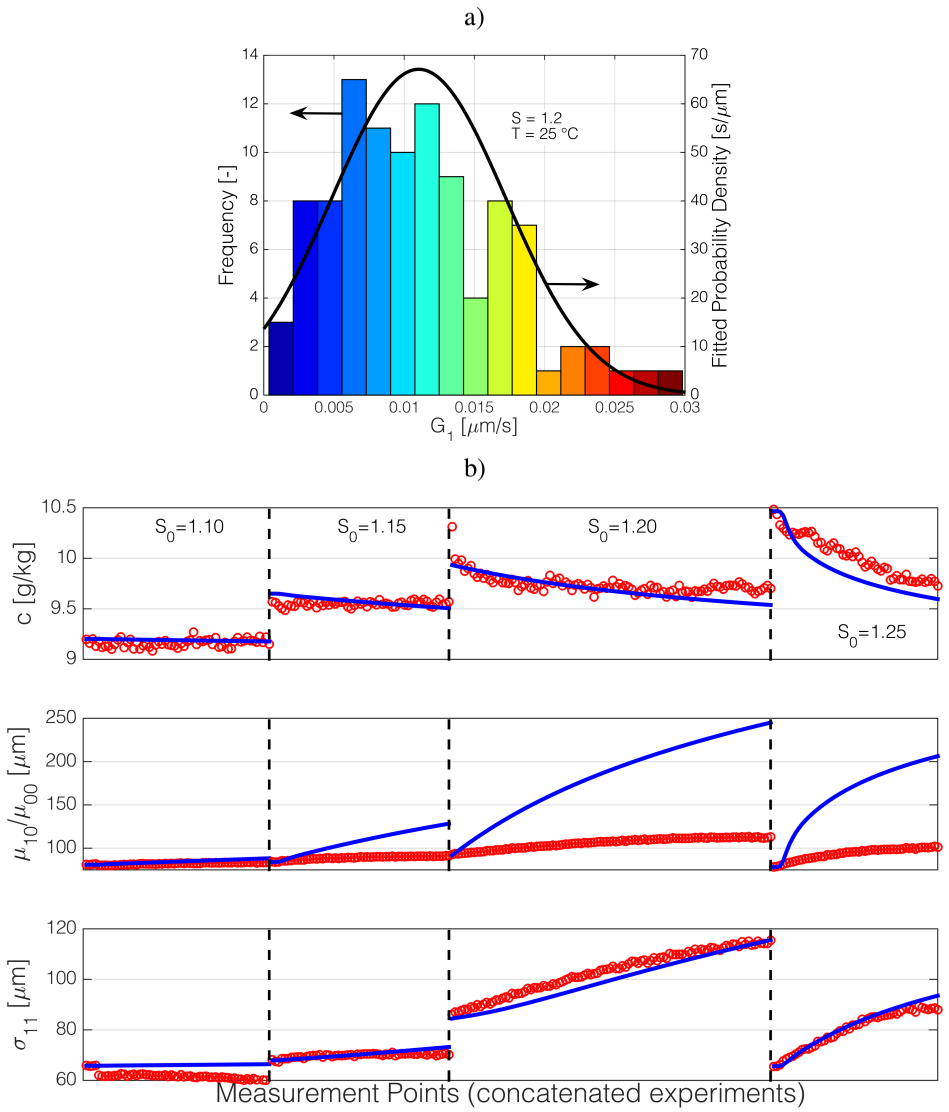

Figure 6: Results of the static *gap* model with no additional degrees of freedom. a) Comparison between measured (single crystal experiments) and fitted growth rate distribution; b) fit result for batch desupersaturation experiments conducted at the same final temperature (concatenated outputs).

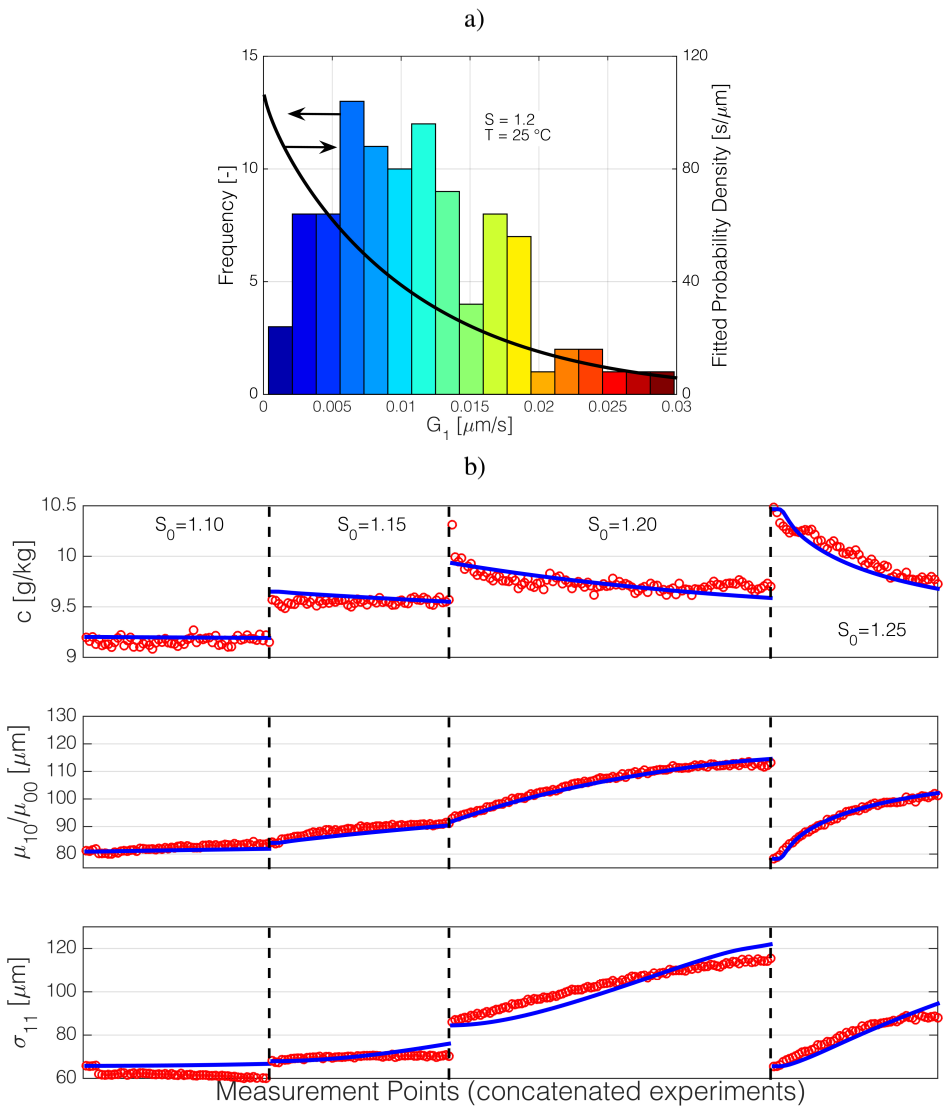

Figure 7: Results of the static *gap* model with parameterized *gap* distribution. a) Comparison between measured (single crystal experiments) and fitted growth rate distribution; b) fit result for batch desupersaturation experiments conducted at the same final temperature (concatenated outputs).

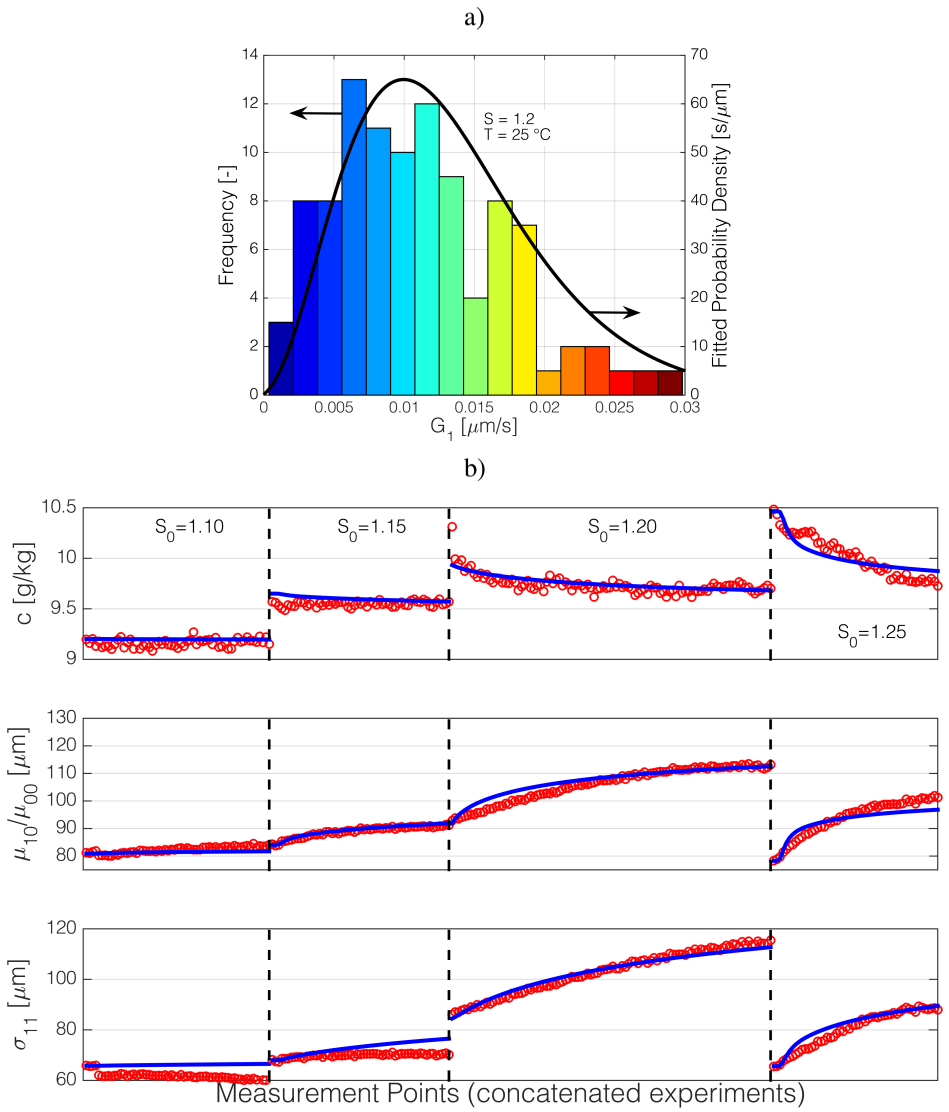

Figure 8: Results of the dynamic *gap* model with no additional degrees of freedom. a) Comparison between measured (single crystal experiments) and fitted growth rate distribution; b) fit result for batch desupersaturation experiments conducted at the same final temperature (concatenated outputs).

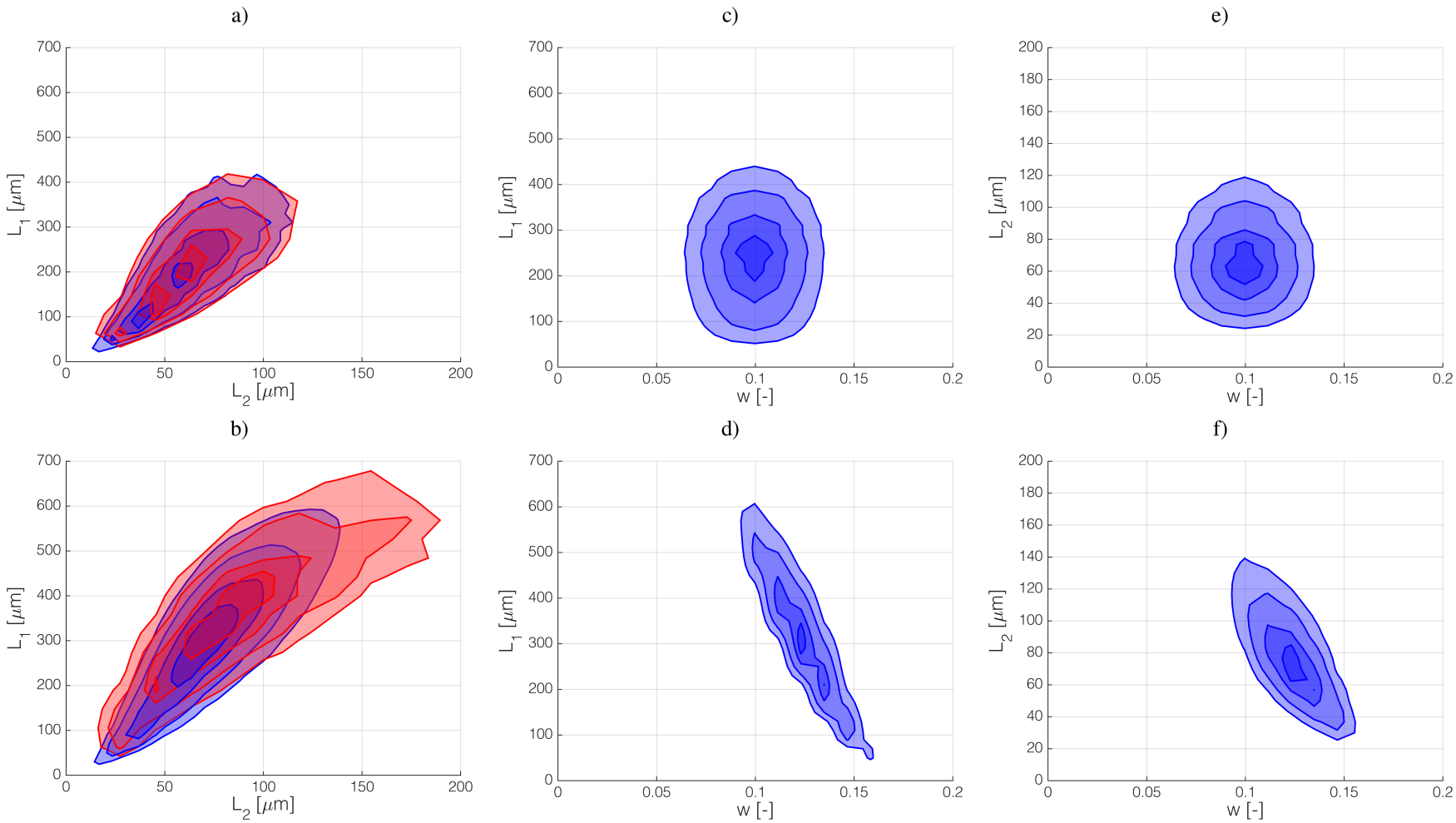

Figure 9: Volume weighted marginal distributions of fitted experiment with $S_0 = 1.20$. a)+b) Initial and final PSSD. Blue contour lines indicate model results while red lines indicate the experimental data; c)+d) Initial and final distributions (projection on L_1 vs. w plane);e)+f) Initial and final distributions (projection on L_2 vs. w plane). All contour lines are drawn at 30%, 50%, 75% and 90% of the respective maximum.

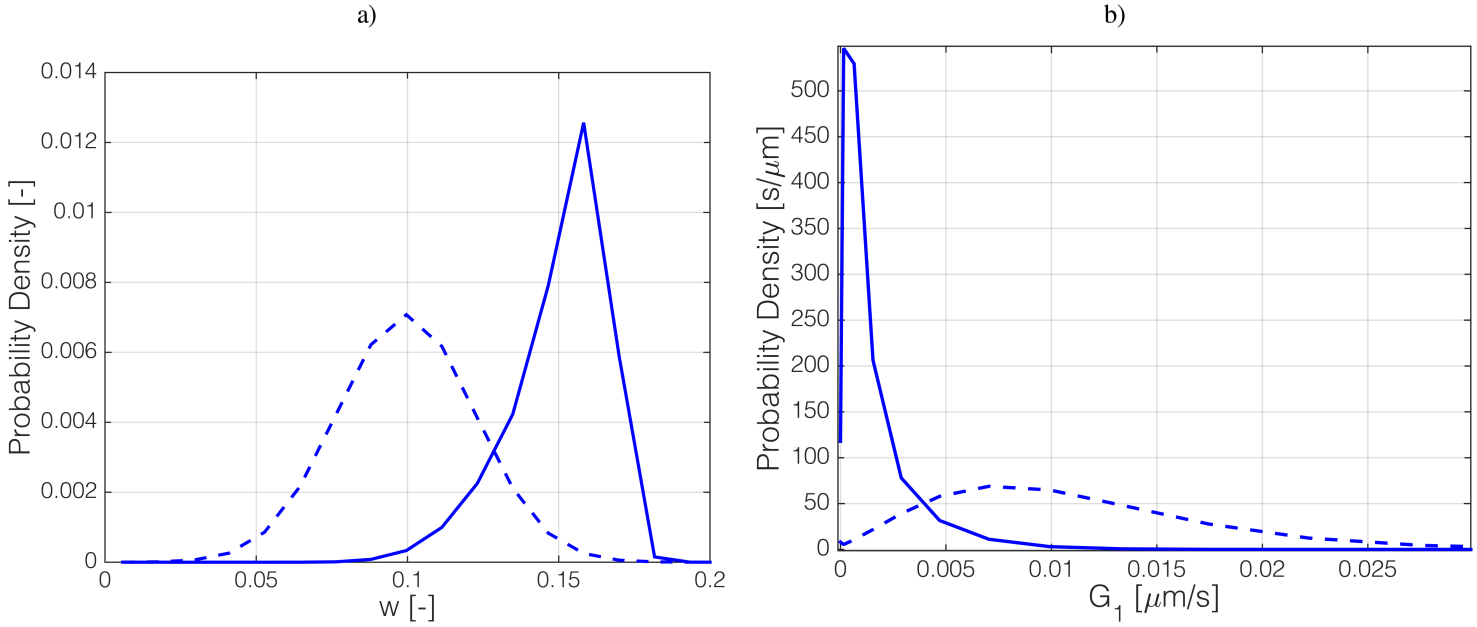

Figure 10: Comparison of the initial (dashed) and final (solid) *gap* and G_1 distribution for the experiment with $S_0 = 1.20$ in the model. a) *gap* distribution; b) growth rate distribution.